An Analysis of Hurricane Opal's Forecast Track Errors Using Quasigeostrophic Potential Vorticity Inversion

JOHN M. HENDERSON*

Department of Atmospheric and Oceanic Sciences, McGill University, Montreal, Quebec, Canada

GARY M. LACKMANN

Department of the Earth Sciences, State University of New York at Brockport, Brockport, New York

JOHN R. GYAKUM

Department of Atmospheric and Oceanic Sciences, McGill University, Montreal, Quebec, Canada

(Manuscript received 16 October 1997, in final form 13 March 1998)

ABSTRACT

Hurricane Opal's landfall in October 1995 forms the basis of a serious hurricane forecast problem—the potential for hurricane conditions over land with insufficient warning time. Official National Hurricane Center (NHC, a division of the Tropical Prediction Center) forecasts predicted landfall and passage inland over the eastern United States at a later time than observed because of underestimation of the northward component of the steering flow by the National Centers for Environmental Prediction's (NCEP) operational models and other hurricane track models. The goal of this paper is to isolate the cause of the poor forecast of meridional storm motion in NCEP's early Eta Model by using quasigeostrophic potential vorticity (QGPV) inversion. QGPV inversion permits decomposition of the steering flow into contributions from different synoptic-scale features.

The inversion procedure is applied to the Eta analysis and 48-h Eta forecast valid at 1200 UTC 5 October 1995. Analyses from the European Centre for Medium-Range Weather Forecasts form an independent comparison for the Eta Model forecasts and analyses. An extratropical cyclone to the northwest of Opal and a synoptic-scale ridge to the east are identified as being major contributors to the steering flow. The Eta Model underpredicted the intensity of the ridge positioned immediately downstream of the storm, resulting in a corresponding underprediction of the meridional steering flow by 5 m s^{-1}.

It is hypothesized that the Eta Model underforecasted the magnitude and extent of Opal's outflow, and subsequent interaction with the downstream ridge, largely due to the model's inability to correctly represent the convection associated with the hurricane in both the analyses and forecasts. Underforecasted upper-tropospheric temperatures downstream of Opal are consistent with this hypothesis. Accurate initialization of the model in the region containing Opal may have been hampered by the dearth of upper-air data over the Gulf of Mexico. Failure to properly resolve the hurricane is hypothesized to have resulted in the underforecasting of the downstream ridge and its associated steering flow.

1. Introduction

Accurate prediction of hurricane motion is crucial for advising disaster officials and the public of the location and timing of dangerous hurricane conditions. A generation has been exposed firsthand to the effects of storms such as Hugo in 1989 and Andrew in 1992, which brought wind gusts of up to 80 m s^{-1} (Willoughby and Black 1996). Consequently, damage estimates in the United States have skyrocketed in recent years, including the $7 billion attributed to Hugo (Case and Mayfield 1990) and $20–$25 billion from Andrew (Mayfield et al. 1994). As a testament to the value of hurricane landfall forecasts by the National Hurricane Center (NHC, a division of the Tropical Prediction Center), the number of hurricane-related fatalities continues to decrease even as the population living in susceptible coastal areas continues to increase significantly (Sheets 1990).

Hurricane Opal in October 1995 emphasized the need for timely NHC track forecasts for two reasons. First, the storm underwent rapid and unexpected intensifica-

* Current affiliation: Atmospheric and Environmental Research, Cambridge, Massachusetts.

Corresponding author address: John M. Henderson, Atmospheric and Environmental Research, 840 Memorial Drive, Cambridge, MA 02139-3794.
E-mail: jmh@aer.com

FIG. 1. Locator map for references in the text.

tion 12 h prior to landfall. The storm's central pressure dropped to 916 hPa with winds of 65 m s^{-1}. These wind speeds classified Opal as a category 4 hurricane (59–70 m s^{-1} winds) on the Saffir–Simpson scale (Simpson 1974). Second, the storm accelerated toward land faster than predicted by numerical guidance. As a result, official NHC forecasts underpredicted the magnitude of Opal's acceleration toward the coastal Gulf of Mexico states (refer to Fig. 1 for geographical references).

The case of Hurricane Opal forms the basis of the most feared hurricane forecast scenario—the potential for intense hurricane conditions along a coastline with inadequate warning. Although Opal weakened to category 3 strength (50–58 m s^{-1} winds) prior to early evening landfall on 4 October 1995 near Pensacola, Florida (see Fig. 2 for the NHC best track), it was still the largest and most intense hurricane to make landfall in the United States during 1995. The numerical guidance, including that of the operational early Eta Model, underestimated the northward motion of Opal through the time of landfall (Fig. 3). Official NHC forecasts valid at 1200 UTC 5 October 1995 were up to 12 h slow with the subsequent storm motion over the eastern United States, in part because of the Eta Model's inability to anticipate the storm's inland acceleration. It is essential to understand the reason for the underestimated northward movement of Opal in order to anticipate possible systematic biases of the forecasted environmental steering flow for the more general case of landfalling hurricanes.

The steering flow has been quantified using a pressure-weighted deep-layer average of the observed composite annular wind and geopotential height fields (Jordan 1952; Miller and Moore 1960; George and Gray 1976; Chan and Gray 1982). It has been estimated that about 80% of the variability in the 24-h position forecasts of Atlantic storms can be explained by environmental steering of the storm (Neumann 1979). Various methods to estimate the steering flow based on vertical

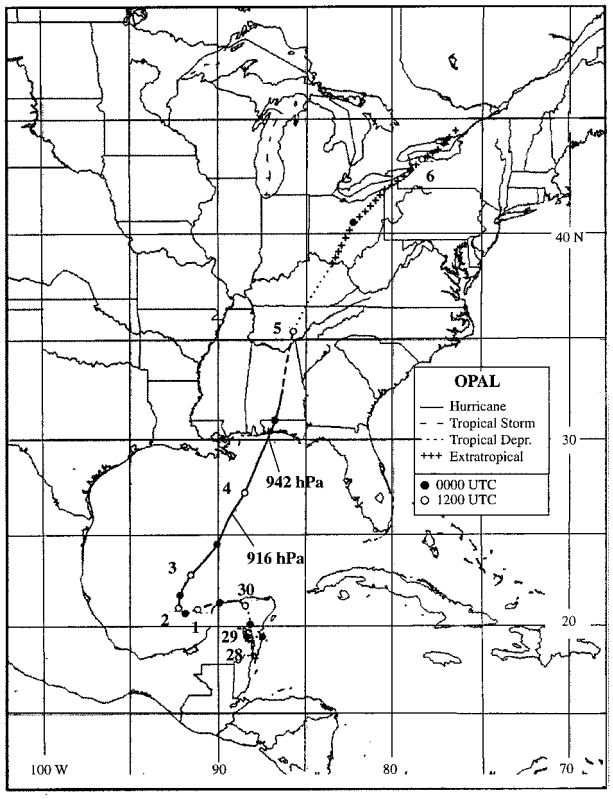

FIG. 2. Best track for Hurricane Opal, 27 September–6 October 1995, adapted from NHC (1995).

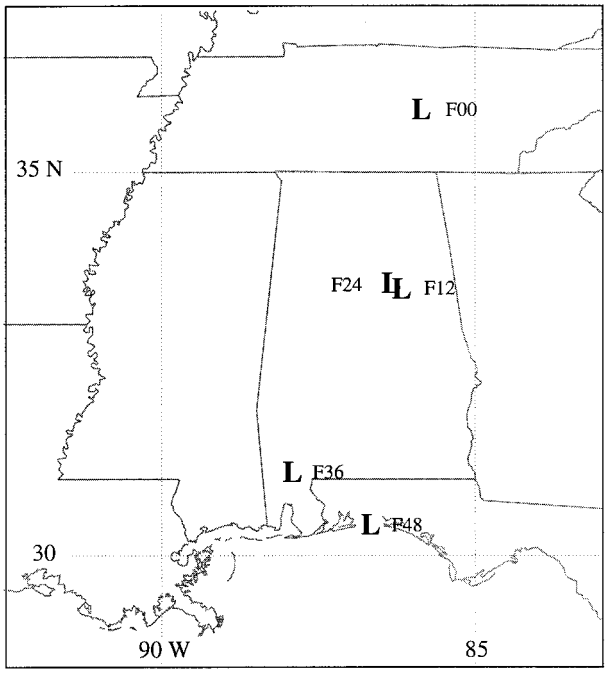

FIG. 3. Eta Model forecast positions of Hurricane Opal valid at 1200 UTC 5 October 1995. The lead times of the position forecasts are given after the letter "F." For example, the 48-h forecast issued at 1200 UTC 3 October is positioned farthest south.

(from 100 hPa to 1000 hPa) and annular (within a 7° lat radius of the composite storm) averages have been shown by George and Gray (1976) and Chan and Gray (1982) to depict storm motion accurately. Individual storms, however, can deviate significantly from these averages, which indicates the need for a method of determining the steering flow that does not rely directly on the geopotential height field near the storm.

Recent potential vorticity (PV) descriptions of the structure and intensity of tropical cyclones (Shapiro and Franklin 1995; Merrill and Velden 1996; Molinari et al. 1995) have been expanded to include hurricane motion and hurricane feedback on the environment. Wu and Emanuel (1995a) present a comprehensive overview of hurricane motion studies and the PV view of hurricane steering. The primary motivation for using PV is the ability to separate and retrieve *individual components* of the hurricane steering flow. The PV approach to describing the hurricane steering flow typically involves piecewise PV inversion and choice of a steering level or vertical deep-layer average of the piecewise wind fields at the center of the hurricane.

As noted by Shapiro (1996), few studies have used the standard Charney (1955) balance equation since it must be linearized if the components of the flow are to sum to the full field. Shapiro (1996) used the near linearity of the asymmetries in the analyses of 1985's Hurricane Gloria and its environment to obtain a steering flow without linearization. The nonlinear terms of the balance equation were assumed to be small.

Wu and Emanuel (1995a,b) used the linearized Charney balance equation (Davis and Emanuel 1991) and piecewise PV inversion (Davis 1992a,b) to describe the hurricane steering flow and hurricane-to-environment interactions for three storms. They defined and quantified the steering flow as the 850–500-hPa balanced flow associated with the entire PV distribution except the positive PV anomaly of the hurricane itself. They observed tropopause lifting (increasing potential temperature on the dynamic tropopause; see Bosart and Lackmann 1995) associated with Hurricane Bob's outflow and the downshear transport of this low PV air. This process has been shown numerically using a simple theoretical model (Wu and Emanuel 1993, 1994) and observations (Wu and Kurihara 1996). Upper-level outflow from a hurricane vortex tilted by vertical shear results in a steering flow to the left of the vertical shear vector (Wu and Emanuel 1993). The PV diagnosis of hurricane steering flow advanced by Wu and Emanuel will be extended in this study by applying the inversion procedure to both analyses and forecasts in an attempt to quantify forecast errors. We, however, invert quasi-geostrophic potential vorticity (QGPV; Charney and Stern 1962; Hoskins et al. 1985, section 5b) to take advantage of its linear operator and efficient inversion procedure. Use of QGPV is appropriate since we are interested in the steering flow associated with synoptic- and larger-scale flows that are only weakly curved in the vicinity of Opal; the representation by QGPV of the hurricane itself is not a primary concern.

TABLE 1. NHC location and 12-h finite difference best-track vector motion for Hurricane Opal.

Date/time	Location	Motion
0000 UTC 4 Oct	24.5°N, 90.1°W	7.2 m s^{-1} from 211°
0000 UTC 5 Oct	31.0°N, 86.8°W	11.3 m s^{-1} from 197°
1200 UTC 5 Oct	35.4°N, 85.7°W	14.8 m s^{-1} from 202°

In this study, we introduce a straightforward QGPV inversion method for obtaining the synoptic-scale steering flow. The poor Eta Model position forecast of Hurricane Opal valid at 1200 UTC 5 October is a notably important hurricane track forecast issue, the understanding of which benefits from the application of our diagnostic method. We apply the QGPV technique at a single time when the Eta Model forecast errors are distinctly observable. Also at this time, Opal is positioned within a robust steering flow that is insensitive to the PV partitioning methodology. Results from 1200 UTC 5 October represent the integrated forecast errors during Opal's recurvature.

We use QGPV inversion to (i) diagnose individual components of the environmental steering flow using European Centre for Medium-Range Weather Forecasts (ECMWF; Simmons 1989; Trenberth 1992) and Eta Model gridded data, and (ii) investigate the cause of the storm's underforecasted northward motion in a robust steering flow by comparing the steering components retrieved from the Eta forecasts to those from model analyses.

A synoptic overview of Hurricane Opal will be presented in section 2. Section 3 details the QGPV inversion technique. The height and geostrophic wind field components retrieved through inversion are presented in section 4 and discussion of the forecast errors and conclusions are presented in section 5.

2. Synoptic overview

a. The life history of Hurricane Opal

The precursor to Opal, Tropical Depression 17, formed at 1800 UTC 27 September 1995 near the east coast of the Yucatan Peninsula of Mexico (Fig. 2) and drifted slowly toward the northern part of the peninsula (Lawrence et al. 1998). The depression was upgraded to Tropical Storm Opal (winds of 18–32 m s^{-1}) at 1200 UTC 30 September and drifted slowly westward for 48 h into the Gulf of Mexico in response to weak steering flow. At 1200 UTC 2 October, coincident with reaching hurricane status (winds above 32 m s^{-1}), the steering flow became more organized and Opal moved to the north then north-northeast (Table 1).

As stated by Lawrence et al. (1998), rapid intensification commenced near 0000 UTC 4 October in association with warmer sea surface temperatures, well-es-

tablished upper-level outflow, and constriction of the eyewall as part of an eyewall replacement cycle (Willoughby et al. 1982). Opal's lowest central pressure of 916 hPa (at about 1000 UTC 4 October) represents a 42-hPa pressure fall over 12 h, making Opal a rapid deepener (defined as a pressure fall of at least 42 hPa in 24 h; Holliday and Thompson 1979).

Landfall occurred at approximately 2200 UTC 4 October in the Florida panhandle east of Pensacola with sustained surface winds of 50 m s^{-1} and a central sea level pressure of 942 hPa. Postlandfall sustained winds weakened as the storm accelerated inland and Opal was downgraded to a tropical storm by 0600 UTC 5 October over central Alabama and to a tropical depression 6 h later. Nine deaths in the United States were attributed to Opal with damage estimates at $3 billion.

b. The synoptic environment

Ertel (1942) PV, to a very high degree of approximation in a hydrostatic atmosphere, is given in isobaric coordinates by

$$\text{EPV} = -g(f + \zeta)\frac{\partial \theta}{\partial p} + g\left(\frac{\partial v}{\partial p}\frac{\partial \theta}{\partial x} - \frac{\partial u}{\partial p}\frac{\partial \theta}{\partial y}\right) \quad (1)$$

and evaluated using ECMWF data. Here g is the gravitational acceleration, f the Coriolis parameter, ζ the relative vorticity evaluated on a constant pressure surface, θ the potential temperature, u and v the respective zonal and meridional components of the observed wind, and p the pressure. ECMWF height and temperature data are available on a 1.125° × 1.125° grid at the following isobaric levels: 1000, 925, 850, 700, 500, 400, 300, 250, 200, 150, 100, 70, and 50 hPa. The gridded data are interpolated onto a 1° × 1° horizontal grid of dimension 121 × 56.

The utility of dynamic tropopause maps for interpretation of synoptic-scale dynamics has been demonstrated in many studies (e.g., Hoskins and Berrisford 1988; Davis and Emanuel 1991; Hakim et al. 1995). We show the distribution of potential temperature on the 1.5 PVU (potential vorticity unit, 10^{-6} m^2 s^{-1} K kg^{-1}) surface. Since EPV is relatively small and uniform in the troposphere relative to the stratosphere, its vertical gradient is concentrated near the tropopause and plots of potential temperature on the dynamic tropopause provide a compact description of upper-tropospheric dynamics. Tropopause potential temperatures (θ_T) are low (high) where the tropopause is at lower (higher) altitudes, such as in a trough (ridge). Furthermore, under adiabatic conditions, local potential temperature changes are due primarily to advection, which makes regions of convection and latent heating readily identifiable. Regions of substantial latent heat release are associated with the appearance of new potential temperature maxima, given a steady environmental field.

Prior to the rapid intensification of the storm and soon after recurvature (Fig. 4a, valid 0000 UTC 4 October), southerly flow between an intensifying extratropical cyclone over Colorado and a high pressure area in the western North Atlantic characterizes the synoptic environment surrounding Opal. The corresponding tropopause map (Fig. 4b) shows a warm tropical air mass (high θ_T) over the southeastern United States bounded to the north by a subtropical jet from northern Mexico to northern Louisiana. The subtropical jet then merges with the polar jet to the northeast. A shortwave trough is embedded in the jet over eastern Missouri.

At 1200 UTC 5 October Opal is embedded in southwesterly flow between the extratropical cyclone to the northwest and the west Atlantic high (Fig. 4c). This low and the Atlantic ridge have both intensified relative to 0000 UTC 4 October, and the ridge has drifted slightly eastward (Fig. 4c). Table 1 shows that Opal maintained a quasi-steady heading for the duration of its northward movement, suggesting that the steering flow was due to slowly changing synoptic features. At upper levels the cyclonic gyre of the western low is now well defined in the central plains and is associated with an extensive area of lower tropopause potential temperature (Fig. 4d). To the east, Opal is located along the western edge of the tropical air that is being advected over the eastern third of the United States. The isolated areas of potential temperature above 370 K at 0000 UTC 4 October have consolidated into an extensive area covering a large part of the southeastern United States (Figs. 4b,d). In the vicinity of Opal, the tropopause potential temperature has increased 14 K over the 36-h period. This tropopause lifting was likely aided by Opal's outflow that was warmed by latent heating. ''Phase locking'' (Molinari et al. 1995) between Opal and the downstream ridge occurred as the storm's outflow advected eastward then northeastward and helped maintain the position and intensity of the ridge.

3. Data and inversion methodology

a. Data

The Eta Model (Mesinger et al. 1988; Black et al. 1993; Black 1994; Rogers et al. 1996) is the earliest operational guidance available from the National Centers for Environmental Prediction (NCEP) and is part of the regional and global numerical model package that is consulted by NHC forecasters (F. Lepore 1997, personal communication). The ''early'' Eta Model fields were obtained from the Unidata Local Data Management system at McGill University. The data are stored on a 93 × 65 point grid on a Lambert Conformal projection, with 50-hPa vertical resolution. The ECMWF data were obtained courtesy of the National Center for Atmospheric Research. The 1200 UTC 5 October ECMWF model analysis forms an independent comparison of the Eta Model analysis at 1200 UTC 5 October and the 48-h Eta forecast issued at 1200 UTC 3

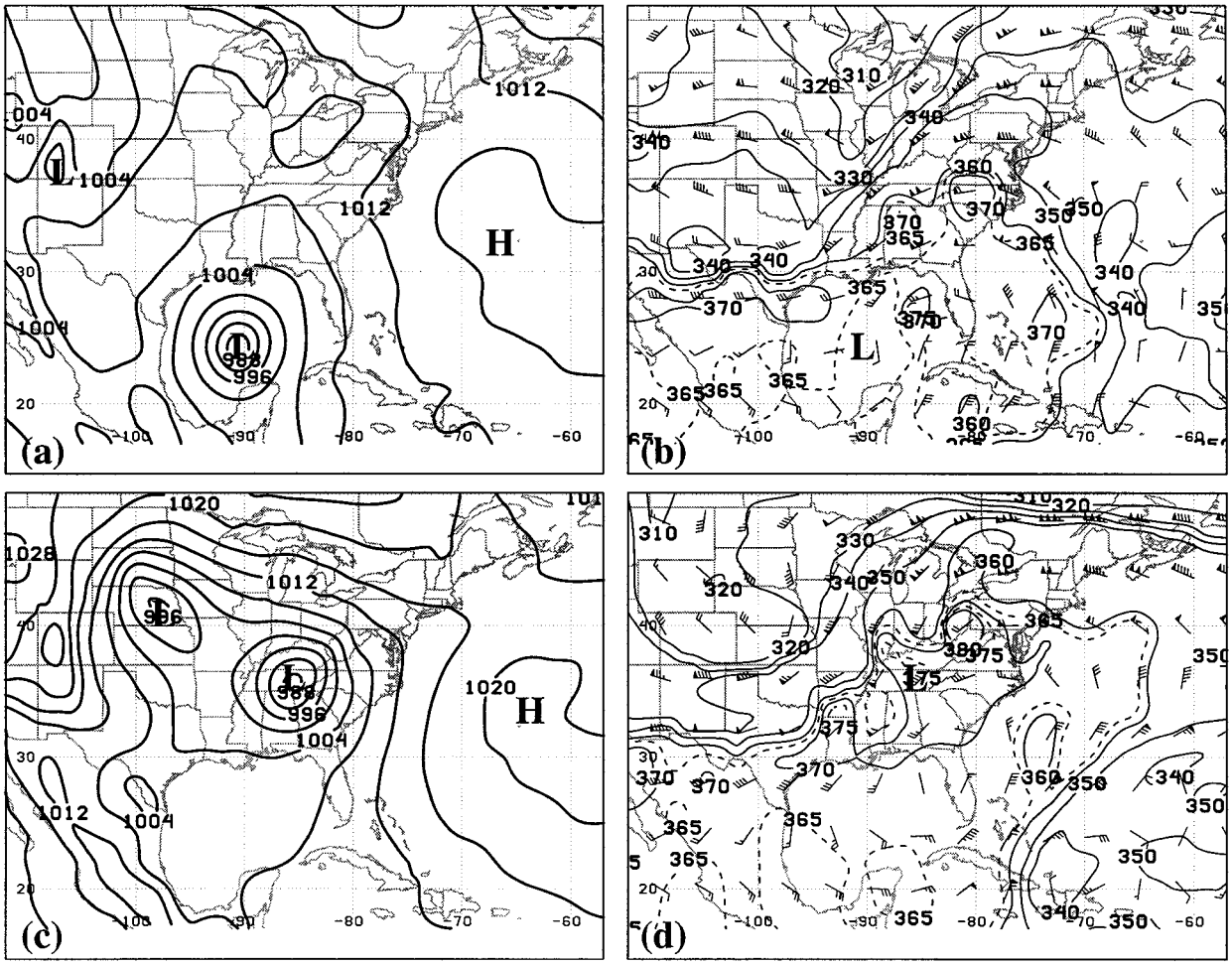

FIG. 4. ECMWF sea level pressure (SLP) and tropopause analyses. (a) and (b) Valid at 0000 UTC 4 October; (c) and (d) valid at 1200 UTC 5 October. (a) and (c) SLP maps (contoured every 4 hPa). (b) and (d) Dynamic tropopause maps depicting potential temperature (solid, every 10 K below 360 K and alternating solid and dashed every 5 K above and including 360 K) and winds (barb = 5 m s^{-1}; pennant = 25 m s^{-1}). Contours of potential temperature above 380 K have been omitted in (d) for clarity. The position of Opal is denoted by the letter "L" in the Gulf of Mexico in (a) and (b) and over Tennessee in (c) and (d). The position of the steering anticyclone is denoted by the "H" in the western Atlantic Ocean in (a) and (c); the position of the steering cyclone is denoted by the "L" over Colorado in (a) and Nebraska in (c).

October. The domains of inversion for the ECMWF and Eta, respectively, are bounded by (10°N, 150°W and 65°N, 30°W) and (12°N, 133°W and 57°N, 49°W).

b. QGPV

QGPV was calculated according to the expression

$$q = \frac{1}{f_o}\nabla^2\phi' + f + f_o\frac{\partial}{\partial p}\left(\frac{1}{\sigma_r}\frac{\partial\phi'}{\partial p}\right), \qquad (2)$$

where ∇^2 is the horizontal Laplacian operator in pressure coordinates, ϕ' the geopotential deviation from an isobarically averaged reference atmosphere (here taken to be the International Civil Aeronautical Organization's Standard Atmosphere), and $f_o = 10^{-4}$ s^{-1}. The static stability coefficient is

$$\sigma_r = -\frac{\alpha}{\theta}\frac{d\theta_r}{dp}, \qquad (3)$$

where θ_r is the potential temperature of the reference atmosphere and α is the specific volume.

c. QGPV inversion procedure

The dynamic and thermodynamic properties of large-scale features can be retrieved through QGPV inversion. Geopotential fields associated with the three-dimensional QGPV distribution can be obtained through numerical inversion of the PV field through use of the geostrophic relation (involving the wind and mass fields) and specified boundary conditions (BCs). The most attractive aspect of PV inversion is the ability to

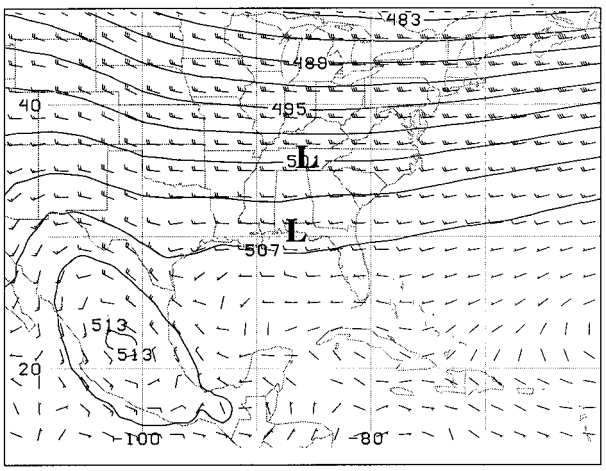

FIG. 5. The CLIMO deep-layer (850–300 hPa) average geopotential height (dam, contoured every 3 dam) and geostrophic wind (same notation as in Fig. 4) fields. The observed and Eta 48-h forecast positions of Opal valid at 1200 UTC 5 October are denoted by the letter "L" over Tennessee and the Florida panhandle, respectively.

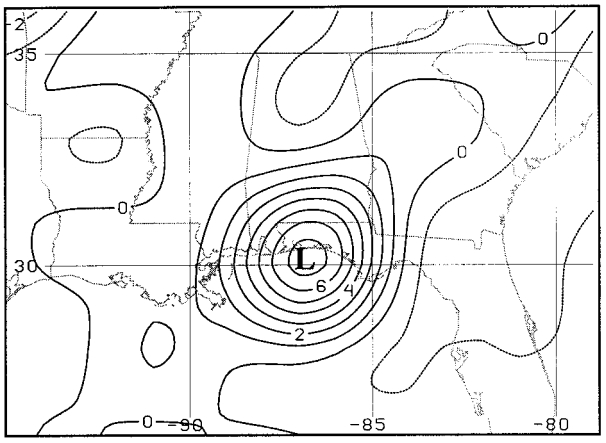

FIG. 6. Lower-tropospheric anomalous QGPV field from ECMWF analysis valid at 0000 UTC 5 October (contoured every 10^{-4} s^{-1}, negative dashed). The position of Opal is denoted by the letter "L."

associate height and wind fields with individual *components* of PV.

The QGPV inversion system used here is based on that of Hakim et al. (1996). QGPV can be written as a linear operator

$$\mathcal{L}[\phi'] = q_* = \left[\frac{1}{f_o}\nabla^2 + f_o\frac{\partial}{\partial p}\left(\frac{1}{\sigma_r}\frac{\partial}{\partial p}\right)\right]\phi', \qquad (4)$$

where $q_* \equiv q - f$. The balanced geopotential fields, ϕ_i', associated with individual partitioned pieces of QGPV, q_{*i}, can be retrieved through numerical inversion of

$$\phi_i' = \mathcal{L}^{-1}[q_{*i}]. \qquad (5)$$

The full QGPV field, $q_* = q - f$, was partitioned into three components (Lackmann and Gyakum 1996; Lackmann et al. 1998). The first is a 10-yr ECMWF October climatology (hereafter CLIMO) compiled by Trenberth (1992) that is largely devoid of synoptic signatures in the region of interest. The second and third are the positive and negative QGPV anomaly fields (hereafter, CYCLO and ANTI, respectively) defined by subtracting the climatological QGPV from the observed field. Partitioning the anomalies by sign permits the identification of wind fields associated with positive and negative QGPV anomalies that have robust circulations at the surface and on the dynamic tropopause (see Fig. 4). The steering flow associated with the extratropical cyclone and the west Atlantic ridge can then be quantified. Since the meridional component of steering flow attributable to CLIMO is small near Opal (Fig. 5), the underforecasted southerly flow is primarily associated with the QGPV anomaly fields, ANTI and CYCLO.

The lower- and middle-tropospheric positive QGPV anomaly associated with Opal [likely formed by PV redistribution through latent heating (see e.g., Bosart and Bartlo 1991; Raymond 1992)] is easily identifiable in the anomaly field (Fig. 6). This anomaly is removed in a manner similar to Wu and Emanuel (1995a,b) by replacing the grid points at every level within the anomaly with the climatological QGPV value (i.e., zero anomaly). Self-advection due to PV asymmetries is removed by this process. The remaining QGPV field is associated with the computed steering flow (Wu and Emanuel 1995a,b). Note that interaction of the hurricane outflow with the environment (see Wu and Emanuel 1993) is retained in the ANTI component. Several test inversions show that the exact definition of the hurricane PV anomaly to be removed (a subjective procedure because of the anomaly's imperfect axisymmetry) had little effect on the inverted flow fields.

As noted by Wu and Emanuel (1995a), use of a long-term climatology (such as their 3-month time mean) instead of a short-term temporally centered climatology (on the order of synoptic timescales) may result in a positive storm anomaly that has little relation to the storm itself (i.e., the shape and magnitude of the storm's anomaly may be significantly influenced by the planetary-scale flow regime rather than by the storm itself). However, the QGPV signature of Opal was relatively compact and isolated from the synoptic features between 0000 UTC 4 October and 1200 UTC 5 October (Fig. 6, valid at 0000 UTC 5 October), which facilitated isolation of the storm's positive QGPV anomaly.

Dirichlet BCs involving the observed distribution of ϕ' are used for the CYCLO (ANTI) lateral and horizontal BCs where this value is negative (positive) on the boundary; elsewhere on the boundary $\phi' = 0$ is specified. A similar methodology is employed by Lackmann et al. (1998). This is a natural choice since the zero geopotential anomaly contour distinguishes between the relative strengths of the geopotential fields associated with the positive and negative QGPV anom-

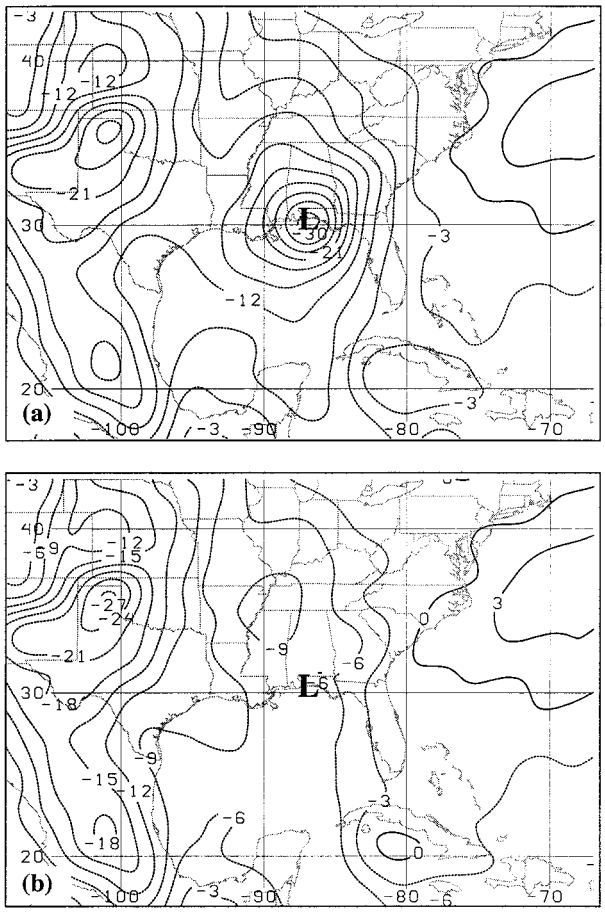

FIG. 7. Lower boundary field (1000 hPa) of anomalous geopotential (contoured every 3×10^2 m^2 s^{-2}) for ECMWF analysis valid at 0000 UTC 5 October: (a) observed and (b) adjusted. The position of Opal is denoted by the letter ''L.''

alies. (Positive and negative QGPV anomalies are associated with negative and positive geopotential anomalies, respectively.) To minimize any further subjectivity in the choice of lateral BCs, the lateral boundaries are placed sufficiently distant so that their effects are small in the vicinity of Opal. See Hakim et al. (1996, section 4) for a detailed investigation of the sensitivity of QGPV inversion to the type of BC used.

The lower (1000-hPa) BC retains the contribution to the steering flow by the synoptic-scale geopotential gradient in the vicinity of Opal. The size and shape of the 1000-hPa negative geopotential anomaly associated with Opal is determined by inverting Opal's positive QGPV anomaly with homogeneous BCs. The boundary reflection of Opal is assumed to have the same structure as the 700-hPa geopotential field associated with Opal's QGPV anomaly. The 1000-hPa field is modified to remove Opal's signature by subtracting a constant multiple of the inverted 700-hPa field. The resulting ''adjusted'' lower BC is smoothly varying and shows little of Opal's circulation (cf. Fig. 7a and Fig. 7b).

Geostrophic winds were then calculated for CYCLO, ANTI, and CLIMO from the geopotential fields and vertically averaged from 850 to 300 hPa following Velden and Leslie (1991) and Velden (1993). They observed that inclusion of the uppermost tropospheric levels can introduce variance into the steering flow; use of the boundary layer makes the inversion procedure more sensitive to the lower BC. Physically, it is advection of the hurricane's tropospheric-deep positive QGPV anomaly that is responsible for the movement of the storm. Our results are not highly sensitive to the definition of the steering flow. To quantify the steering flow components, we then horizontally average the deep-layer wind fields over the domain of Opal's tropospheric QGPV anomaly.

4. Results

The geostrophic steering flow obtained through PV inversion is now presented for 1200 UTC 5 October. This time was chosen for several reasons: 1) The 48-h Eta forecast valid at this time exhibited the largest position error for Opal, 2) Opal was located well within the U.S. surface and upper-air network, increasing the likelihood of representative model analyses, 3) the synoptic pattern remained relatively constant from 0000 UTC 4 October to 1200 UTC 5 October, and 4) the inversion results were similar to earlier times.

a. ECMWF and Eta analyses

Figure 8a shows the deep-layer steering flow associated with FULL (defined as the sum of CLIMO, CYCLO, and ANTI) for the ECMWF analysis valid at 1200 UTC 5 October. The deep-layer geopotential height field in Fig. 8 is the vertical average of the geopotential heights every 50 hPa from 850 to 300 hPa. The inversion procedure retrieves the expanding and intensifying southwesterly flow (results for 0000 UTC 4 October are not shown but cf. Fig 8a with Table 1 and Figs. 4a and 4c). Opal is located in the center of a broad southwesterly steering flow between a well-formed cyclonic gyre over Nebraska (central height less than 477 dam) and an anticyclonic gyre east of Cape Hatteras (central height more than 522 dam). The deep vertical extent of the gyres facilitates identification of these synoptic-scale steering features. The features have become more organized over the past 36 h (not shown) with the ridge having built more than 6 dam. (Note that the position of these anomalous deep-layer circulations need not be collocated with the surface features seen in Fig. 4c.)

The anomalies, CYCLO and ANTI (Figs. 8b and 8c, respectively), contribute significantly to the advective flow—about 50% of the total retrieved flow—including most of the meridional component. The southerly flow associated with CYCLO is largely due to the extratropical cyclone to Opal's northwest. In contrast, ANTI is steering Opal to the northwest in response to large-scale

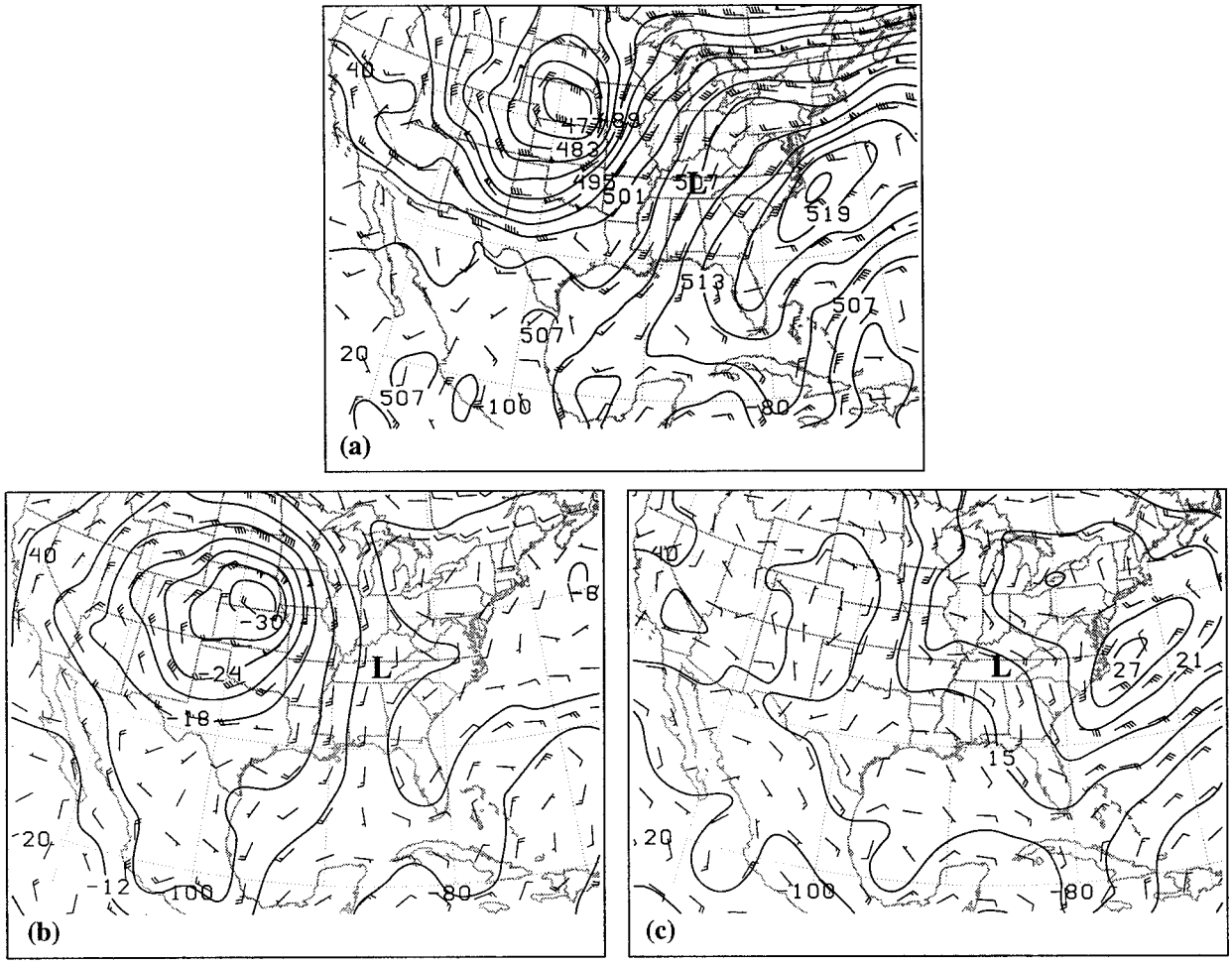

FIG. 8. Deep-layer steering flow and wind field for the 1200 UTC 5 October ECMWF analysis. (a) The FULL geopotential height field (sum of Figs. 5, 8b, and 8c) in dam and geostrophic winds (same notation as in Fig. 4). (b) and (c) The CYCLO and ANTI components, respectively. Opal's position is denoted by the ''L'' over Tennessee.

ridge building along the U.S. east coast and Florida. Heights over the Great Lakes have risen more than 8 dam over 36 h (not shown). Two distinct anticyclonic gyres are seen, though the elongated gyre off the mid-Atlantic states is dominant.

The flow fields associated with FULL, CYCLO, and ANTI from the 1200 UTC 5 October Eta Model analysis (Figs. 9a, 9b, and 9c, respectively) again show a broad southwesterly flow over Opal, though the circulation to the east of Opal in Fig. 9a is fragmented and weaker by about 9 dam. The CYCLO-associated flow in Fig. 9b is qualitatively similar to that of Fig. 8b in the vicinity of Opal. However, a significantly weaker upper low in the Bahamas (Fig. 9b) appears to diminish the easterly flow in the western Atlantic that contributes to the region's less-robust anticyclonic circulation (cf. Fig. 9a with Fig. 8a). The maximum height anomaly associated with ANTI (Fig. 9c) is weaker by about 3 dam though the overall effect on the steering flow is similar. The gyre closest to Opal (positioned over Ohio) is steering the storm to the northwest while in the ECMWF analysis the Great Lakes' high pressure cell is likely preventing Opal from rounding the western edge of the ridge.

We now define a vector-difference quantification of each fractional contribution to the steering flow by a particular QGPV component,

$$\text{fractional contribution} = 1 - \frac{|\mathbf{X} - \mathbf{OBS}|}{|\mathbf{OBS}|}, \quad (6)$$

where **X** is the vector obtained from the inversion procedure (e.g., the flow associated with ANTI) and **OBS** is the observed motion vector of Opal. Thus, the fractional contribution equals unity for each component only when the component vector and **OBS** are equal. The quantitative steering contributions, expressed as a percentage of **OBS**, by CYCLO and ANTI in the vicinity of Opal for the ECMWF analysis (Fig. 10a) are similar to those from the Eta analysis (Fig. 10b). The QGPV inversion procedure is successful in retrieving 85%

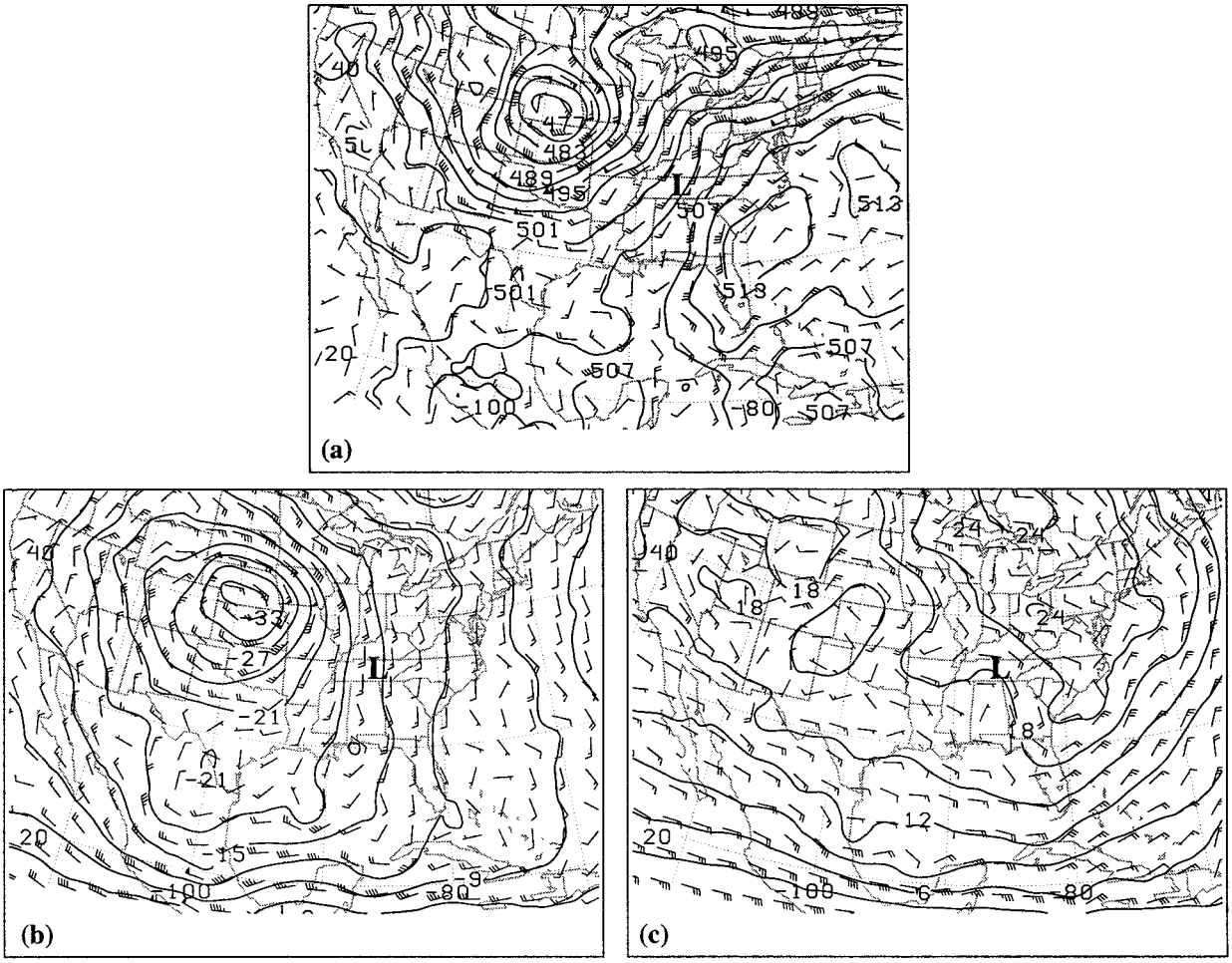

FIG. 9. As in Fig. 8 except for the Eta analysis valid at 1200 UTC 5 October. Opal's position is denoted by the L over Tennessee.

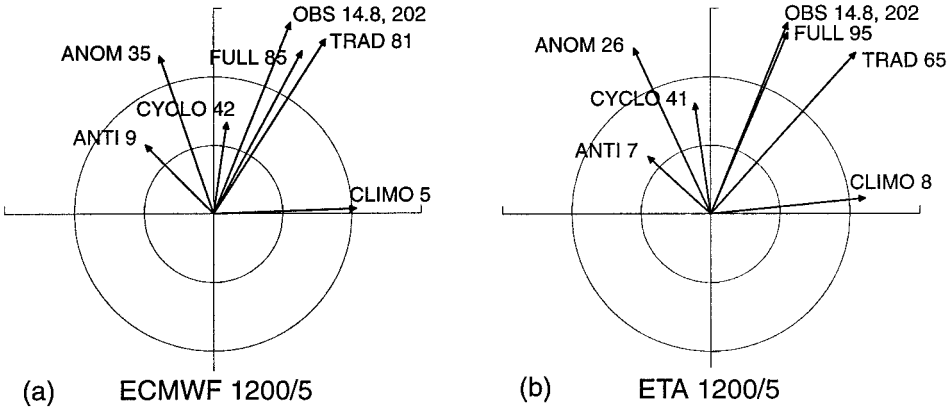

FIG. 10. Vector plots of the components of the steering flow for 1200 UTC 5 October for the (a) ECMWF analysis and (b) Eta analysis, corresponding to Figs. 8 and 9, respectively. Averaging is from 850 to 300 hPa over the domain of Opal's positive QGPV anomaly. Numbers are the vector-difference contributions of each component to the steering flow expressed as a percentage of the vector **OBS** (m s^{-1} and degrees). Inner (outer) concentric circle represents winds of 5 m s^{-1} (10 m s^{-1}).

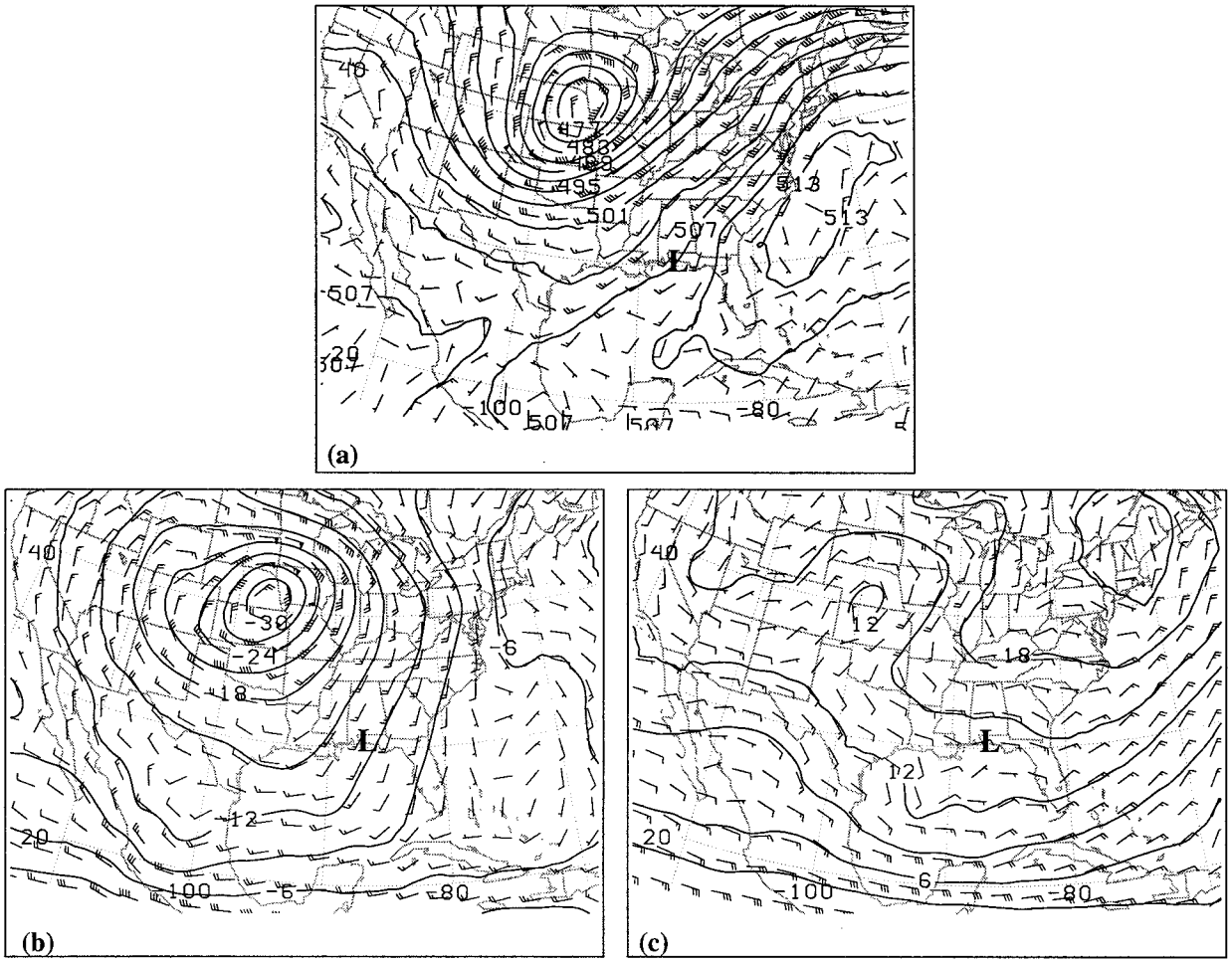

FIG. 11. As in Fig. 8 except for the 48-h Eta forecast valid at 1200 UTC 5 October. Opal's position is denoted by the "L" over the Florida panhandle.

(ECMWF) and 95% (Eta) of **OBS**. The average contribution (ECMWF and Eta data) by CYCLO, ANTI, and CLIMO is 41%, 8%, and 6%, respectively, whereas the anomalies (the sum of ANTI and CYCLO; hereafter denoted by ANOM) contribute 30%. The difference in CLIMO between the ECMWF (5%) and Eta (8%) models is attributable to the Eta's placement of Opal slightly farther north in the midlatitude westerlies (more distant from the NHC's position than the ECMWF's analysis) and slight model differences in the shape and size of Opal's positive QGPV anomaly. Included for reference is a traditional (hereafter TRAD) 5°–7° lat annular average of the observed height fields, which retrieves 81% of **OBS** using the ECMWF model data, but only 65% in the Eta Model because it exhibits an eastward bias.

b. Eta Model forecasts

The FULL flow from the 48-h Eta forecast valid at 1200 UTC 5 October (Fig. 11a) shows that the most significant difference between the forecast and analyses is the intensity and location of the anticyclonic circulation to the north and east of Opal (cf. Figs. 8a and 9a). Ridging northwest into Ohio through Lake Superior and a closed anticyclonic gyre over central Ontario in Fig. 9a is absent in the 48-h forecast and has been replaced by a weak trough. The stronger intensity of the western low (Fig. 11b) compared to the Eta analysis (Fig. 9b) does not affect the CYCLO contribution in the vicinity of Opal. Of significance, however, is Fig. 11c, which shows *a weaker and significantly more distant ridge.* The center of the ridge is now distant from Opal over New England and the coastal ridge is absent (cf. Fig. 8c). Heights are up to 8 dam lower over the Great Lakes. *The weaker and more distant ridge contributes a largely zonal (easterly) flow from ANTI over Opal.* The misforecasted position of Opal is largely a consequence of the loss of significant southerly steering flow.

The quantitative flow contributions for the 48-h Eta forecast (Fig. 12) show that ANTI has decreased to −15%. The negative value indicates that the vector difference between **OBS** and ANTI is of greater magnitude

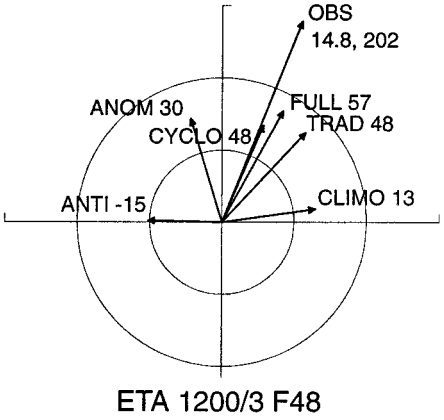

FIG. 12. As in Fig. 10 except for the 48-h Eta forecast valid at 1200 UTC 5 October, corresponding to Fig. 11.

than the magnitude of **OBS**. ANTI decreased over the forecast cycle (i.e., from the 12 to the 24, 36 then 48-h forecasts) valid at 1200 UTC 5 October and was negative for the forecasts of longer than 12 h. The poor representation of the eastern ridge compared to the analyses results in the loss of a large contribution to the steering flow, including a substantial meridional component, from ANTI. Consequently, for the 48-h forecast valid at 1200 UTC 5 October, FULL can retrieve only 57% of the observed storm motion though ANOM (30%) remains similar to the analyses' values. The ability of TRAD to retrieve only 48% shows that traditional methods of determining the flow perform poorly due to their dependence on proper modeling of the height field in the vicinity of Opal.

The decrease in ANTI is the only trend symptomatic of the Eta Model's decreasing ability to represent the eastern ridge at longer forecast lead times. The change in CLIMO is a consequence of Opal being forecasted progressively farther south; Opal was forecasted to be making landfall in the Florida panhandle in the 48-h forecast. CLIMO contributes only a zonal flow and so cannot itself advect Opal farther north.

It is significant that the shorter-lead time Eta forecasts are similar to the Eta analysis in developing a more robust eastern ridge. The pronounced ridge in the ECMWF analysis is consistent with what is expected downstream of a powerful hurricane, suggesting that this analysis is more representative of actual conditions. Furthermore, the ECMWF analysis has a later data cutoff time of +3 h (Escoffier and Provost 1995) compared to the Eta Model's +1.25 h (Rogers et al. 1995), which allows for early dissemination. We may then critically consider the synoptic representation of the 1200 UTC 5 October Eta analysis as being an improvement over the Eta forecasts, yet exhibiting errors common to the forecasts.

5. Concluding discussion

The purpose of this paper is to determine the cause of the Eta Model's underforecasted steering flow for Hurricane Opal. We identify two synoptic-scale features—an extratropical cyclone to the west of Opal and a synoptic-scale ridge to the east—as contributing significantly to Opal's steering flow. We demonstrate the value of piecewise QGPV inversion in decomposing the flow into contributions from the positive and negative QGPV anomaly fields. The ''missing'' steering flow is present in the anticyclonic downstream ridge contribution in the ECMWF and Eta analyses. The eastern ridge is progressively weaker and placed more distant from Opal in the earlier Eta forecasts valid at 1200 UTC 5 October.

The less-developed eastern ridge at the large forecast lead times results in a significant loss of steering flow. The vector difference between the 48-h Eta forecast of ANTI w.r.t. the ECMWF analysis is 4.8 m s^{-1} from 182°. By taking the vector differences between the 12-, 24-, 36-, and 48-h ANTI forecasts, respectively, and the ECMWF ANTI analysis, integrating over 12-h periods and summing, the total ANTI forecast error is 709 km along the vector 352° (to the north). Considering that the 48-h forecast error displacement is 576 km oriented along 190° from the forecasted position, the missing flow advects Opal to a position 240 km west-northwest (304°) of the NHC-analyzed position. This indicates that the poor representation of the downstream ridge (and the associated weaker ANTI contribution) *alone* can fully explain the meridional component of the missing flow, though with a westward bias.

The reduction in flow is a consequence of major differences in the magnitude and positioning of the eastern ridge w.r.t. Opal. The absence of Opal forming the distinct upstream edge to the ridge, owing to the lack of strong ridging immediately east and northeast of Opal, leads one to suspect that processes occurring in the vicinity of Opal played a major role in the model errors. *We hypothesize that the Eta Model failed to predict the magnitude and extent of Opal's outflow with subsequently less downstream ridge development.* The effects of the loss of storm outflow have been shown in a case study by Ross and Kurihara (1995) for Hurricane Gloria. The ridge downstream of the storm was more intense and positioned closer to the storm when Gloria was included in their numerical study compared to model runs without the storm.

This form of storm-to-environment modification occurs when the region of low-PV outflow air, formed above a mature hurricane in response to PV redistribution by latent heating (Bosart and Bartlo 1991), is advected downstream by the upper-level flow. There are two main thermodynamic and dynamic consequences. First, the outflow builds the downstream ridge by warming the upper troposphere at distances far greater than the extent of the storm's near-surface effects (Davis et al. 1993; Morgan 1996; Stoelinga 1996). Second, an anticyclonic circulation offset downstream from the center of the cyclonic storm circulation forms in association with the upper-level negative PV anomaly (Wu and

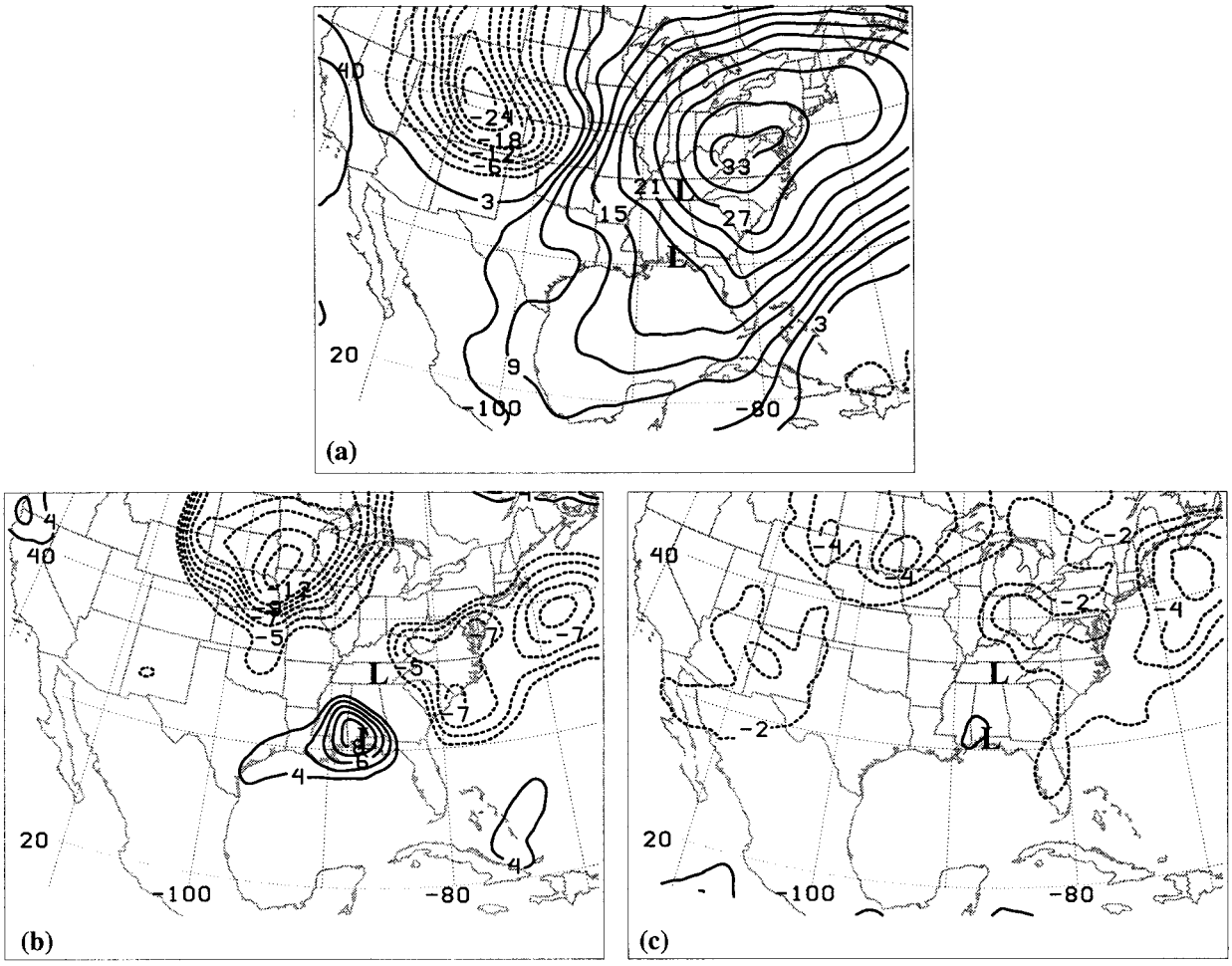

FIG. 13. Observed Eta Model thickness anomalies and forecast errors (forecast minus observed): (a) observed Eta 850–300-hPa thickness anomaly field at 1200 UTC 5 October (contoured every 3 dam), (b) 48-h forecast error of 850–300-hPa thickness (contoured every 1 dam for errors of magnitude greater than 3 dam), and (c) 48-h forecast error of ANTI upper-level (500–300 hPa) thickness (contoured every 1 dam for errors of magnitude greater than 1 dam). The northern ''L'' is the 1200 UTC 5 October analyzed position of Opal; the southern ''L'' is the 48-h forecasted position.

Emanuel 1993, 1994). The interaction between a storm's lower-level PV maximum and upper-level PV minimum was seen observationally by Wu and Kurihara (1996). They found that the downstream upper-level negative PV anomaly contributed 3 m s^{-1} of steering flow to the motion of Hurricane Bob. The ANTI forecast error of approximately 5 m s^{-1} found in this study is largely related to the presence in the analyses of an intimately positioned ridge to the east and northeast of Opal that is likely due to hurricane outflow. The southerly steering flow associated with this feature (the ridge immediately downstream of Opal in Figs. 8c and 9c) combined with the easterly flow from the distant preexisting ridge (over New England in Fig. 11c) to produce a southeasterly steering flow.

Investigation of the thickness forecast errors supports the notion of underforecasted outflow. The observed thickness anomaly field from 850 to 300 hPa (Fig. 13a) shows a highly amplified thermal pattern at 1200 UTC 5 October. The main feature is a massive warm anomaly centered immediately northeast of the observed position of Opal. The diffluent upper-level flow is west-southwesterly in the vicinity of Opal, then westerly and northerly farther downstream as part of the anticyclonic gyre on the tropopause (Fig. 4d). The pattern of tropopause winds suggests that air from the vicinity of Opal is being advected directly into the downstream ridge. As expected, the forecast error field of 48-h 850–300 hPa anomalous thickness (Fig. 13b) shows a large area of negative error (up to 8 dam, approximately 5.5°C) immediately downstream of Opal, extending into the western Atlantic. (The positive anomaly collocated with Opal's forecasted position is associated with Opal's poor phase speed forecast; the negative anomaly just northeast of Nebraska is associated with the poor phase speed forecast of the extratropical cyclone.) Furthermore, Fig. 13c shows that the upper-level 500–300-hPa layer contributes significantly to the forecast error. In the vicinity

of the ANTI-associated anticyclonic gyre over Ohio (Fig. 9c), upper-level thicknesses are underforecasted by more than 3 dam (approximately 2°C). Lower-tropospheric temperatures were warmer than forecast along the Florida coast, which may also contribute to underestimation of the ridge amplitude in the model forecast.

The insufficient storm outflow in the Eta Model is likely due to several factors. The most obvious and important is the failure of the Eta Model (as well as other synoptic-scale models) to resolve the intensity and structure of the storm. The 80-km resolution of the early Eta Model in October 1995 simply cannot capture in any detail the features of a hurricane. For example, the 12-hourly Eta Model analyses valid from 1200 UTC 3 October to 1200 UTC 5 October underestimated Opal's sea level pressure by 21, 33, 58, 27, and 6 hPa (the latter value followed landfall). During the period that encompassed the storm's rapid intensification of 49 hPa (and a subsequent weakening of 63 hPa), the analyzed Eta (ECMWF) sea level pressure dropped only 12 (7) hPa to a minimum of 977 (982) hPa. The Eta forecast sea level pressures originating from these runs deepened Opal to only 982 hPa (the 12-h forecast valid at 0000 UTC 5 October) and were up to 70 hPa too weak (24-h forecast valid 1200 UTC 4 October).

The model's inability to analyze and forecast the storm's convectively driven low central pressures is partly a consequence of model resolution and the need to parameterize the physics involved. Explicit modeling of the complex multiscale interactions, ranging from synoptic to cloud scales, that determine the structure and intensity of tropical systems is only now being attempted (Liu et al. 1997). Dickinson et al. (1997) also showed that modeling of large-scale cyclogenesis (in this case the 12–14 March 1993 superstorm) can suffer from insufficient parameterized cumulus convection and related upper-level outflow. A coarse-scale analysis very likely is responsible for poor forecasted intensities and missed occurrences of rapid intensification. Unexpected rapid intensification (as in the case of Opal) may lead

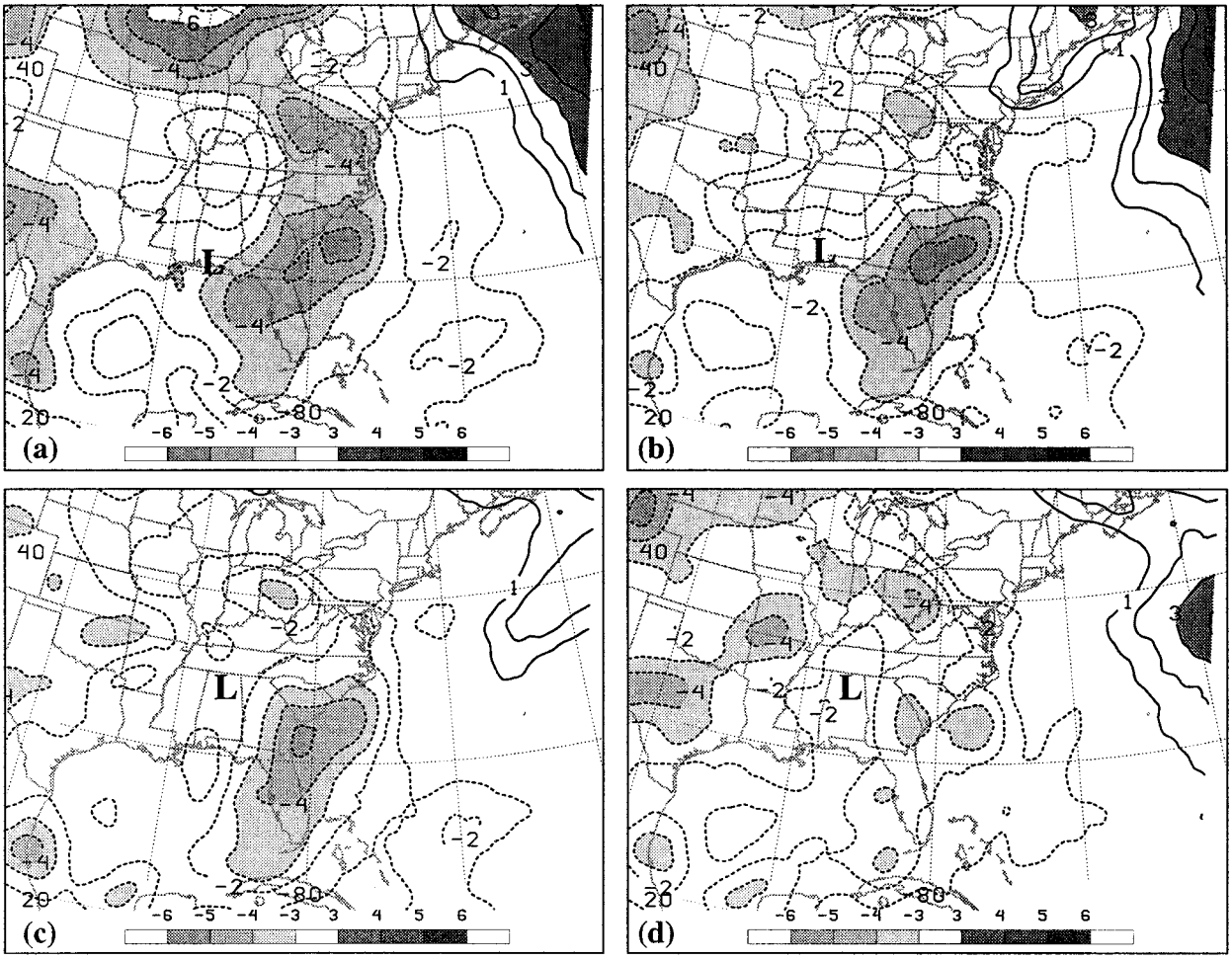

FIG. 14. Eta forecast errors (forecast minus observed) of deep-layer (850–300 hPa) geopotential heights for the (a) 48-h, (b) 36-h, (c) 24-h, and (d) 12-h forecasts valid at 1200 UTC 5 October. The contour interval is 1 dam. The zero contour has been omitted for clarity. The forecasted position of Opal is indicated in each panel by "L."

to significantly underforecasted outflow and unforecasted influences on storm track after sufficient time for the outflow to be advected downstream (K. Emanuel 1997, personal communication). Only after a storm makes landfall and strong eyewall convection weakens does the importance of a poor intensity analysis and subsequent forecast lessen.

The effects of the upper-tropospheric outflow, however, may be hard to quantify because of poor resolution of the initial upper-level data. Compounding the problem are model data quality control algorithms that reject isolated outlying, but representative, data reports as being erroneous (K. Emanuel 1997, personal communication). Data resolution is of greatest concern when the hurricane is located in a data sparse area, such as the Gulf of Mexico. It is significant that the largest improvement in ANTI (i.e., the largest percentage increase of steering flow contribution) occurred with the 0000 UTC 5 October Eta run, both for data valid at 0000 UTC 5 October (the analysis) and 1200 UTC 5 October (the 12-h forecast). Figure 14 shows the improving representation of the downstream ridge with these later model runs. The expansive negative forecast errors (indicative of underforecasted heights) in the downstream ridge along the southeast U.S. coast and Florida (Figs. 14a and 14b) decrease in magnitude (to about 3 dam) and extent with later model runs (Figs. 14c and 14d). This indicates large-scale ridge building is being captured by the model at later times, especially by the 0000 UTC 5 October run (Fig. 14d, the 12-h forecast). The greatest improvement coincides closely with storm landfall. Therefore by 0000 UTC 5 October, the storm center, and perhaps more importantly the upper-level outflow, were being advected over the relatively dense surface and upper-air network of the U.S. southeast.

It is hoped that increased horizontal model resolution, such as the upgrade of the early Eta Model to 48 km in 1995 (Mesinger 1996) and to 32 km in 1998 (Mittelstadt 1998), will improve the ability to resolve the details of tropical systems, though only with increased raw data input. We stress the need for improved upper-level data observation, such as the use of dropwindsondes (Burpee et al. 1996; Tuleya and Cord 1997) and aircraft (Langford and Emanuel 1993; Shapiro 1996), in the vicinity of tropical systems and in neighboring synoptic features subject to modification by the storm. As well, the implementation into numerical models of wind fields retrieved from satellites is expected to improve tropospheric analyses and hurricane track forecasts (Velden et al. 1992; Velden 1996; Velden et al. 1997).

We note the application of our technique to real-time hurricane forecasting. Hurricane steering mechanisms can be simply and quickly quantified from standard model output, which may identify and resolve model (and forecaster) disagreements and aid in pattern recognition and forecast evaluations. Applied to many historical case studies, our technique may detect systematic differences in forecast track errors among various models that can be attributed to varying horizontal and vertical resolution, physical parameterizations, and input data sources. Future research, in general, must continue to identify these forecast errors common to both operational NCEP and NHC hurricane models in order to further improve hurricane track forecasts.

Acknowledgments. This work is based on the first author's M.Sc. thesis. We thank Dr. Greg Hakim of the University at Albany, State University of New York (current affiliation the National Center for Atmospheric Research) for providing the QGPV inversion code. We acknowledge ECMWF and NCAR for providing the ECMWF analyses and climatological field, and the Local Data Manager and UNIDATA for providing the Eta Model data. This research was funded in part by a Natural Science and Engineering Research Council of Canada Research Grant and by its postgraduate scholarship awarded to John Henderson. Additional support for this research was provided by the Canadian Institute for Climate Studies, the Atmospheric Environment Service of Canada, and NSF Grant ATM-9707443, awarded to the State College of New York at Brockport. Comments from two anonymous reviewers substantially improved the manuscript; reviewer A suggested a valuable method for representing the steering flow. Greg Hakim also provided valuable comments that improved the final manuscript. We thank Marco Carrera, Alex Fischer, and Neil Montgomery for improving the text of the manuscript and Mr. Carrera also for help in printing the final manuscript.

REFERENCES

Black, T. L., 1994: The new NMC mesoscale Eta Model: Description and forecast examples. *Wea. Forecasting,* **9,** 265–278.

——, D. G. Deaven, and G. J. DiMego, 1993: The step-mountain Eta-coordinate model: 80 km ''early'' version and objective verifications. NWS Tech. Proc. Bull. 412, National Oceanic and Atmospheric Administration/National Weather Service, 31 pp. [Available from National Weather Service, Office of Meteorology, 1325 East–West Highway, Silver Spring, MD 20910.]

Bosart, L. F., and J. A. Bartlo, 1991: Tropical storm formation in a baroclinic environment. *Mon. Wea. Rev.,* **119,** 1979–2013.

——, and G. M. Lackmann, 1995: Postlandfall tropical cyclone reintensification in a weakly baroclinic environment: A case study of Hurricane David (September 1979). *Mon. Wea. Rev.,* **123,** 3268–3291.

Burpee, R. W., J. L. Franklin, S. J. Lord, R. E. Tuleya, and S. D. Aberson, 1996: The impact of Omega dropwindsondes on operational hurricane track forecast models. *Bull. Amer. Meteor. Soc.,* **77,** 925–933.

Case, B., and M. Mayfield, 1990: Atlantic hurricane season of 1989. *Mon. Wea. Rev.,* **118,** 1165–1177.

Chan, J. C.-L., and W. M. Gray, 1982: Tropical cyclone movement and surrounding flow relationships. *Mon. Wea. Rev.,* **110,** 1354–1374.

Charney, J. G., 1955: The use of primitive equations of motion in numerical prediction. *Tellus,* **7,** 22–26.

——, and M. E. Stern, 1962: On the stability of internal baroclinic jets in a rotating atmosphere. *J. Atmos. Sci.,* **19,** 159–172.

Davis, C. A., 1992a: Piecewise potential vorticity inversion. *J. Atmos. Sci.,* **49,** 1397–1411.
——, 1992b: A potential-vorticity diagnosis of the importance of initial structure and condensational heating in observed extratropical cyclogenesis. *Mon. Wea. Rev.,* **120,** 2409–2428.
——, and K. A. Emanuel, 1991: Potential vorticity diagnostics of cyclogenesis. *Mon. Wea. Rev.,* **119,** 1929–1953.
——, M. T. Stoelinga, and Y.-H. Kuo, 1993: The integrated effect of condensation in numerical simulations of extratropical cyclogenesis. *Mon. Wea. Rev.,* **121,** 2309–2330.
Dickinson, M. J., L. F. Bosart, W. E. Bracken, G. J. Hakim, D. M. Schultz, M. A. Bedrick, and K. R. Tyle, 1997: The March 1993 superstorm cyclogenesis: Incipient phase synoptic- and convective-scale flow interaction and model performance. *Mon. Wea. Rev.,* **125,** 3041–3072.
Ertel, H., 1942: Ein neuer hydrodynamischer Wirbelsatz. *Meteor. Z.,* **59,** 277–281.
Escoffier, C., and C. Provost, 1995: Wind forcing over the southwest Atlantic: Comparison between observations and ECMWF analyses. *Mon. Wea. Rev.,* **123,** 1269–1287.
George, J. E., and W. M. Gray, 1976: Tropical cyclone motion and surrounding parameter relationships. *J. Appl. Meteor.,* **15,** 1252–1264.
Hakim, G. J., L. F. Bosart, and D. Keyser, 1995: The Ohio Valley wave-merger cyclogenesis event of 25–26 January 1978. Part I: Multiscale case study. *Mon. Wea. Rev.,* **123,** 2663–2692.
——, D. Keyser, and L. F. Bosart, 1996: The Ohio Valley wave-merger cyclogenesis event of 25–26 January 1978. Part II: Diagnosis using quasigeostrophic potential vorticity inversion. *Mon. Wea. Rev.,* **124,** 2176–2205.
Holliday, C. R., and A. H. Thompson, 1979: Climatological characteristics of rapidly intensifying typhoons. *Mon. Wea. Rev.,* **107,** 1022–1034.
Hoskins, B. J., and P. Berrisford, 1988: A potential vorticity perspective of the storm of 15–16 October 1987. *Weather,* **43,** 122–129.
——, M. E. McIntyre, and A. W. Robertson, 1985: On the use and significance of isentropic potential vorticity maps. *Quart. J. Roy. Meteor. Soc.,* **111,** 877–946.
Jordan, E. S., 1952: An observational study of the upper wind-circulation around tropical storms. *J. Meteor.,* **9,** 340–346.
Lackmann, G. M., and J. R. Gyakum, 1996: Heavy cold-season precipitation in the northwestern United States: Climatology and a diagnosis of the flood of 17–18 January 1986. Preprints, *15th Conf. on Weather Analysis and Forecasting,* Norfolk, VA, Amer. Meteor. Soc., 265–268.
——, ——, and R. Benoit, 1998: Moisture transport diagnosis of a wintertime precipitation event in the Mackenzie River Basin. *Mon. Wea. Rev.,* **126,** 668–691.
Langford, J. S., and K. A. Emanuel, 1993: An unmanned aircraft for dropwindsonde deployment and hurricane reconnaissance. *Bull. Amer. Meteor. Soc.,* **74,** 367–375.
Lawrence, M. B., B. M. Mayfield, L. A. Avila, R. J. Pasch, and E. N. Rappaport, 1998: Atlantic hurricane season of 1995. *Mon. Wea. Rev.,* **126,** 1124–1151.
Liu, Y., D.-L. Zhang, and M. K. Yau, 1997: A multiscale numerical study of Hurricane Andrew (1992). Part I: Explicit simulation and verification. *Mon. Wea. Rev.,* **125,** 3073–3093.
Mayfield, M., L. Avila, and E. N. Rappaport, 1994: Atlantic hurricane season of 1992. *Mon. Wea. Rev.,* **122,** 517–538.
Merrill, R. T., and C. S. Velden, 1996: A three-dimensional analysis of the outflow layer of Supertyphoon Flo (1990). *Mon. Wea. Rev.,* **124,** 47–63.
Mesinger, F., 1996: Improvements in quantitative precipitation forecasts with the Eta regional model at the National Centers for Environmental Prediction: The 48 km upgrade. *Bull. Amer. Meteor. Soc.,* **77,** 2637–2649.
——, Z. I. Janjic, S. Nickovic, D. Gavrilov, and D. G. Deaven, 1988: The step-mountain coordinate: Model description and performance for cases of Alpine lee cyclogenesis and for a case of an Appalachian redevelopment. *Mon. Wea. Rev.,* **116,** 1493–1518.
Miller, B. I., and P. L. Moore, 1960: A comparison of hurricane steering levels. *Bull. Amer. Meteor. Soc.,* **41,** 59–63.
Mittelstadt, J., 1998: The Eta-32 model. NWS Western Region Tech. Attachment 98-03, National Oceanic and Administration/National Weather Service, 7 pp. [Available from National Weather Service Western Region Headquarters, Room 1311, 125 S. State St., Salt Lake City, UT 84138-1102.]
Molinari, J., S. Skubis, and D. Vollaro, 1995: External influences on hurricane intensity. Part III: Potential vorticity structure. *J. Atmos. Sci.,* **52,** 3593–3606.
Morgan, M. C., 1996: On the dynamics of diabatically generated ''outflow'' during cyclogenesis. Preprints, *Seventh Conf. on Mesoscale Processes,* Reading, United Kingdom, Amer. Meteor. Soc., 29–31.
Neumann, C. J., 1979: On the use of deep-layer mean geopotential height fields in statistical prediction of tropical cyclone motion. Preprints, *Sixth Conf. on Probability and Statistics in Atmosphere Sciences,* Banff, AB, Canada, Amer. Meteor. Soc., 32–38.
NHC, 1995: Hurricane Opal Preliminary Report. 14 pp. [Available from National Hurricane Center, 11691 S.W. 17th St., Miami, FL 33165-2149.]
Raymond, D. J., 1992: Nonlinear balance and potential-vorticity thinking at large Rossby number. *Quart. J. Roy. Meteor. Soc.,* **118,** 987–1015.
Rogers, E., D. G. Deaven, and G. J. DiMego, 1995: The regional analysis system for the operational Eta Model: Original 80 km configuration and recent changes. *Wea. Forecasting,* **10,** 810–825.
——, T. L. Black, D. G. Deaven, G. J. DiMego, Q. Zhao, M. Baldwin, N. W. Junker, and Y. Lin, 1996: Changes to the operational ''early'' Eta analysis/forecast system at the National Centers for Environmental Prediction. *Wea. Forecasting,* **11,** 391–413.
Ross, R. J., and Y. Kurihara, 1995: A numerical study on influences of Hurricane Gloria (1985) on the environment. *Mon. Wea. Rev.,* **123,** 332–346.
Shapiro, L. J., 1996: The motion of Hurricane Gloria: A potential vorticity diagnosis. *Mon. Wea. Rev.,* **124,** 2497–2508.
——, and J. L. Franklin, 1995: Potential vorticity in Hurricane Gloria. *Mon. Wea. Rev.,* **123,** 1465–1475.
Sheets, R. C., 1990: The National Hurricane Center—Past, present, and future. *Wea. Forecasting,* **5,** 185–232.
Simmons, A. J., 1989: ECMWF medium-range prediction models development of the numerical formulation and the impact of increased resolution. *Meteor. Atmos. Phys.,* **40,** 28–60.
Simpson, R. H., 1974: The hurricane disaster potential scale. *Weatherwise,* **27,** 169–186.
Stoelinga, M. T., 1996: A potential vorticity-based study of the role of diabatic heating and friction in a numerically simulated baroclinic cyclone. *Mon. Wea. Rev.,* **124,** 849–874.
Trenberth, K. E., 1992: Global analyses from ECMWF and atlas of 1000 to 10 mb circulation statistics. NCAR Tech. Note NCAR/TN-373 + STR, 191 pp. [Available from NCAR, P.O. Box 3000, Boulder, CO 80307.]
Tuleya, R. E., and S. J. Cord, 1997: The impact of dropwindsonde data on GFDL hurricane model forecasts using global analyses. *Wea. Forecasting,* **12,** 307–323.
Velden, C. S., 1993: The relationship between tropical cyclone motion, intensity and the vertical extent of the environmental steering layer in the Atlantic basin. Preprints, *20th Conf. on Hurricanes and Tropical Meteorology,* San Antonio, TX, Amer. Meteor. Soc., 31–34.
——, 1996: Winds derived from geostationary satellite moisture channel observations: Applications and impact on numerical weather prediction. *Meteor. Atmos. Phys.,* **60,** 37–46.
——, and L. M. Leslie, 1991: The basic relationship between tropical cyclone intensity and the depth of the environmental steering layer in the Australian region. *Wea. Forecasting,* **6,** 244–253.
——, C. M. Hayden, W. P. Menzel, J. L. Franklin, and J. Lynch,

1992: The impact of satellite-derived winds on numerical hurricane track forecasting. *Wea. Forecasting,* **7,** 107–118.

——, ——, S. J. Nieman, W. P. Menzel, S. Wanzong, and J. S. Goerss, 1997: Upper-tropospheric winds derived from geostationary satellite water vapor observations. *Bull. Amer. Meteor. Soc.,* **78,** 173–195.

Willoughby, H. E., and P. G. Black, 1996: Hurricane Andrew in Florida: Dynamics of a disaster. *Bull. Amer. Meteor. Soc.,* **77,** 543–549.

——, J. A. Clos, and M. G. Shoreibah, 1982: Concentric eye walls, secondary wind maxima, and the evolution of the hurricane vortex. *J. Atmos. Sci.,* **39,** 395–411.

Wu, C. C., and K. A. Emanuel, 1993: Interaction of a baroclinic vortex with background shear: Application to hurricane movement. *J. Atmos. Sci.,* **50,** 62–76.

——, and ——, 1994: On hurricane outflow structure. *J. Atmos. Sci.,* **51,** 1995–2003.

——, and ——, 1995a: Potential vorticity diagnostics of hurricane movement. Part I: A case study of Hurricane Bob (1991). *Mon. Wea. Rev.,* **123,** 69–92.

——, and ——, 1995b: Potential vorticity diagnostics of hurricane movement. Part II: Tropical Storm Ana (1991) and Hurricane Andrew (1992). *Mon. Wea. Rev.,* **123,** 93–109.

——, and Y. Kurihara, 1996: A numerical study of the feedback mechanisms of hurricane–environment interaction on hurricane movement from the potential vorticity perspective. *J. Atmos. Sci.,* **53,** 2264–2282.